Supporting Information for

Control of Molecular Packing toward Lateral Microresonator for Microlaser Array

Xue Jin,[a] Han Huang,[b] Xuedong Wang,[c] Qing Liao,[b] Wenping Hu, *, [a] and Hongbing Fu*[,a,b]

[a] Tianjin Key Laboratory of Molecular Optoelectronic Sciences, Department of Chemistry, School of Sciences, Tianjin University, and Collaborative Innovation Center of Chemical Science and Engineering (Tianjin), Tianjin 300072, P. R. China.

[b] Beijing Key Laboratory for Optical Materials and Photonic Devices, Department of Chemistry, Capital Normal University, Beijing 100048, P. R. China.

[c] Institute of Functional Nano & Soft Materials (FUNSOM) Jiangsu Key Laboratory for Carbon-Based Functional Materials & Devices, Soochow University, Suzhou, Jiangsu, 215123, , P. R. China.

E-mail: hongbing.fu@tju.edu.cn; huwp@tju.edu.cn

Keywords: organic semiconductor laser; molecular packing; lateral microresonator; microlaser array; *Hj*-aggregation

A. Experimental Details.

The Synthesis Route of 6M-DSB Organic Molecule.

All starting materials were purchased from Sigma-Aldrich and used as received without further purification.

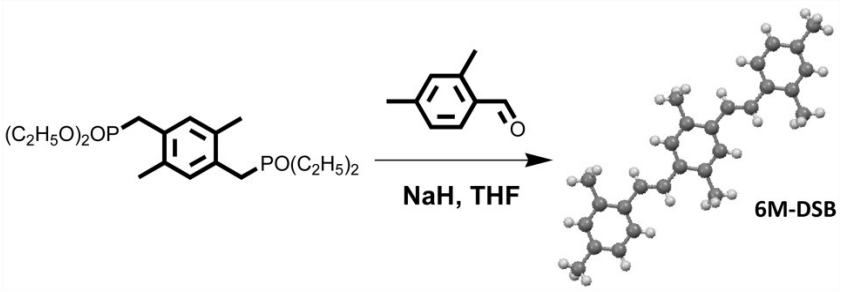

To a mixture of 2,5-dimethyl-1,4-xylene-bis(diethyl phosphonate) (0.81 g, 2.0 mmol) and the 2,4-dimethylbenzaldehyde (0.54 g, 4.0 mmol) in THF cooled in an ice bath was added 2 eq. NaH in small portions during a 30 min period. The reaction mixture was stirred at room temperature for 3 h and poured into water. The phase was extracted with CH_2Cl_2. The pooled organic phases were washed with water, dried over anhydrous $MgSO_4$, filtered, and evaporated. The product was separated by flash chromatography on silica gel by means of CH_2Cl_2/petroleum ether (1:4). Finally a highly fluorescent powder was obtained as the title compound (0.62 g, 1.7 mmol) in 85% yield. ^{1}H NMR (400 MHz, $CDCl_3$): δ7.51 (d, 2 H), 7.42 (s, 2 H), 7.18 (d, 4 H), 7.04 (d, 4 H), 2.43 (s, 6 H), 2.42 (s, 6 H), 2.34 (s, 6 H). ESI-HRMS: Calcd. For $[M+H]^+$: 367.5430. Found: 367.5376. Elemental Anal.: C, 91.82; H, 8.18.

Structural Characterization of Microribbons.

The X-ray diffraction (XRD) patterns were measured by a D/max 2400 X-ray diffractometer with Cu Kα radiation (λ = 1.54050 Å) operated in the 2θ range from 3° to 40°, by using the samples of microribbons filtered on the surface of an AAO membrane.

Fluorescence images were recorded using an Olympus research inverted system microscope (FV1000-IX81, Tokyo, Japan) equipped with a charge couple device (CCD, Olympus DP71, Tokyo, Japan) camera. The excitation source is a Xenon lamp equipped with a band-pass filter (330–380 nm for UV-light). The samples were prepared by placing a drop of dispersion onto a cleaned quartz slide.

B. AFM Measurements of 6M-DSB Organic Microribbons.

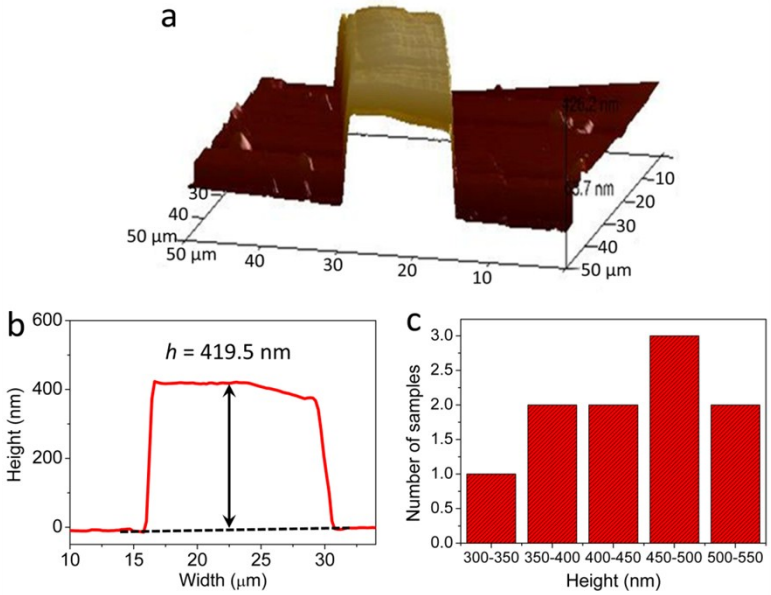

Figure S1A. (a) Atomic force microscopy (AFM) images and corresponding height profiles of one sample 6M-DSB microribbon. (b) The histogram of thickness distribution of microribbons, by randomly measuring the AFM profiles of 10 samples on a quartz substrate. The height (*h*) of the 6M-DSB microribbons ranges from 300 to 550 nm.

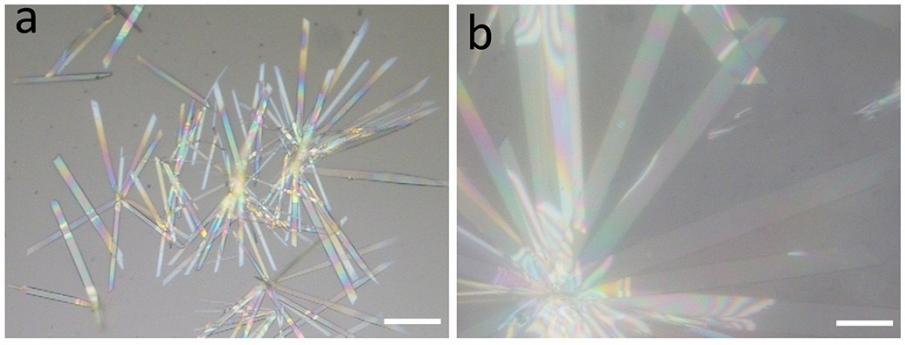

Figure S1B. Bright-field optical microscopic image of microribbons with tunable sizes obtained by dropwise addition of (a) 3 mL of ethanol (W = 5-10 µm) and (b) 2 mL of ethanol (W = 15-30 µm) into 0.1 mL of a stock solution (10 mM) of 6M-DSB dissolved in dichloromethane (DCM). Scale bar: 50 µm.

C. Single Crystal Structure Characteristic.

Table S1.Crystallographic data of 6M-DSB single crystal

Sample	6M-DSB
empirical formula	$C_{28}H_{30}$
molecule weight	366.54
crystal system	monoclinic
space group	P -1
cell dimensions:	
a, Å	4.7533(10)
b, Å	5.9928(12)
c, Å	18.235(4)
α, deg	96.08(3)
β, deg	96.46(3)
γ, deg	90.15(3)
V, Å^3	513.178
Z, Z'	*Z*: 1, *Z'*: 0
R-Factor *(%)*	17.38
crystal size, mm^3	1.50×0.30×0.20

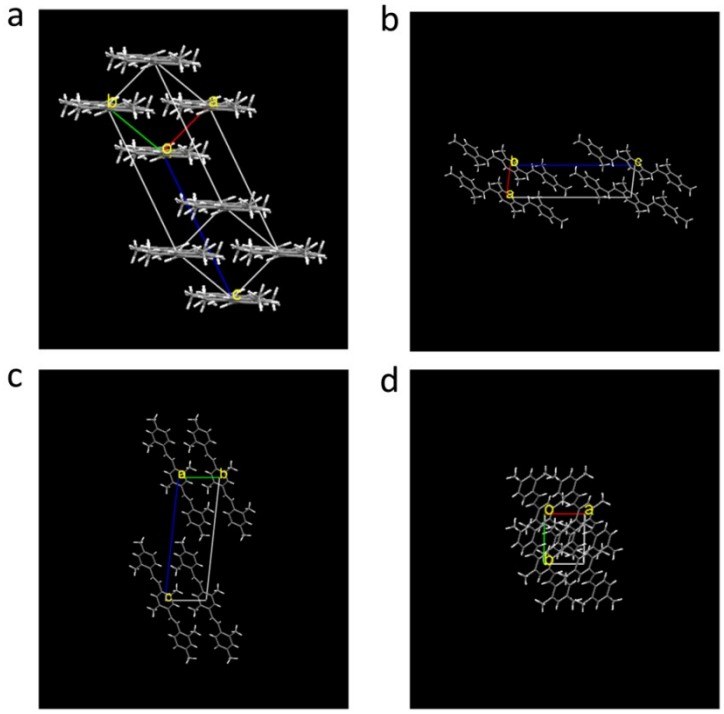

Figure S2. a) Crystal structure of 6M-DSB single crystal. b) View down crystallographic *a* axis. c) View down crystallographic *b* axis. d) View down crystallographic *c* axis.

D. Photophysical Properties of 6M-DSB Solution and Microribbons.

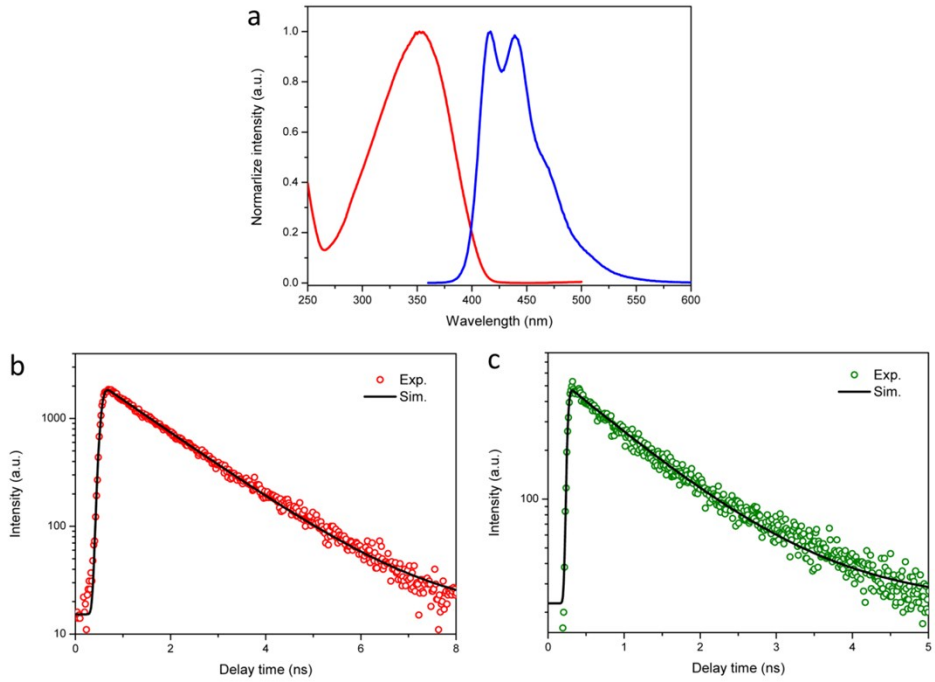

Figure S3. (a) Absorption (blue line) and fluorescence (red line) spectra of 6M-DSB molecules in THF solution with a concentration of 10^{-5} M. (b) and (c) Fluorescence decay profiles of 6M-DSB monomers in THF solution (red, $\tau_{momomer}$ ~ 1.23 ns) and ensemble microribbons (green, τ_{ribbon} ~ 0.60 ns).

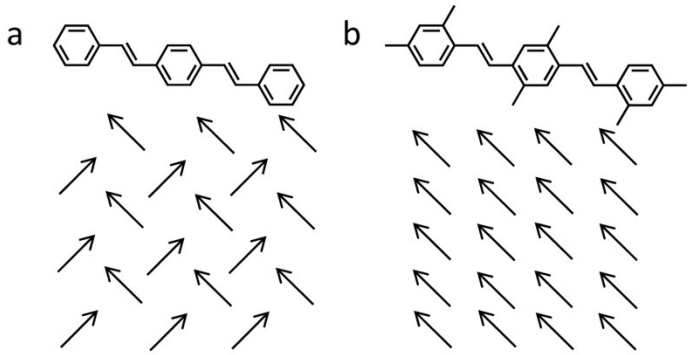

Figure S4. (a) The herringbone-aggregate of DSB single crystal. (b) The uniaxial molecular aggregate of 6M-DSB.

Ref: F. C. Spano, *J. Chem. Phys.* 2003, **118**, 981.

E. Calculation of Energy Transfer Coupling of 6M-DSB

1. Coupling Calculation

1.1 Method

We used the energy splitting method[1] to calculate the coupling between neighbored molecules, which works well for identical molecular dimer. This method will include the coupling from Förster (Coulomb) mechanism and Dexter (exchange) mechanism both, where the later component will be missed by dipole-dipole interaction method or transition density cube method. So when the intermolecular distance is small, this method will be more reliable.

For large molecular distance, the coupling was calculated by dipole-dipole interaction method.[2]

The calculation is based on the TDDFT calculation at CAM-B3LYP/6-311+g* level. After calculation of the dimer, whether the absorption peak is red or blue shifted will determine the coupling is negative or positive, or the aggregate effect is J- or H- style.

1.2 H-aggregate at *ab* direction

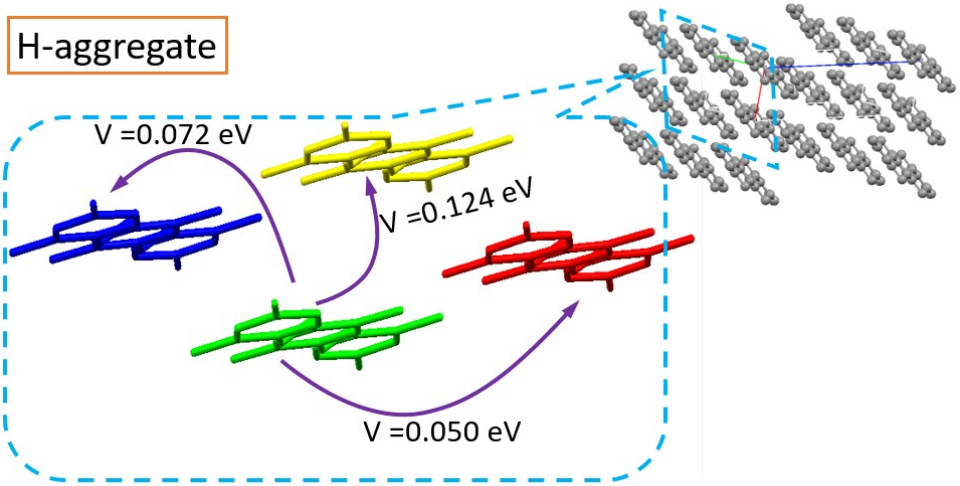

Figure S5. The calculated coupling along ab direction.

1.3 J-aggregate at c direction

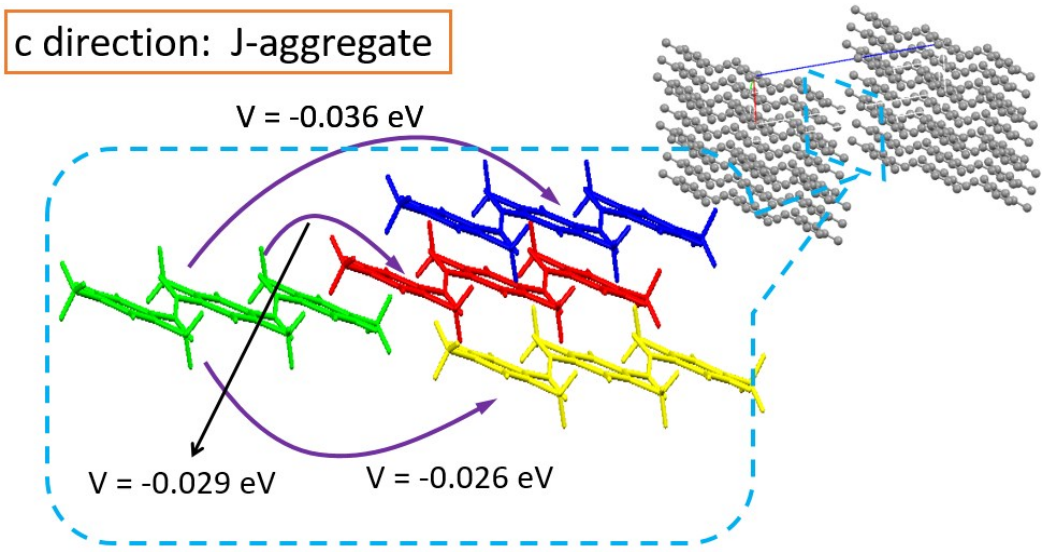

Figure S6. The calculated coupling along c direction.

1.4 Conclusion of Coupling

The coupling inside the *ab* layer is positive and results in the H-aggregate effect, while the coupling along the *c* direction is negative, and leads to J-aggregate. This result agrees with the classic picture of H/J-aggregate, that head-to-end structure →→ is a J-aggregate, and parallel structure C is a H-aggregate. However, the coupling strength for H-aggregate effect is obviously larger than the J-aggregate effect, so the H-aggregate effect will be dominant.

2. Simulation of Absorption and Emission Spectra

The absorption and emission spectra of aggregates were simulated using vibronic exciton theory under two-particle approximation.[3-4] The necessary parameters were obtained from the simulation of the spectra of separated molecules in solution.

2.1 Simulation of spectra in solution without aggregation

The spectra of molecular spectra without aggregation is determined by several parameters of the molecule: (1) excitation energy ε; (2) solvent shift D_{sol}; (3) vibrational frequency ω; (4) Huang-Rhys factor λ^2; (5) excited state relaxation energy before emission ε_{relax}; (6) absorption/emission band broadening width σ_{abs} and σ_{em}. By fitting the experimental spectra, we obtained the parameters as following: $(\varepsilon + D_{sol})=27451\ cm^{-1}$; $\omega=1200\ cm^{-1}$; $\lambda^2=1.12$; $\varepsilon_{relax} = 3397\ cm^{-1}$; $\sigma_{abs} = 950\ cm^{-1}$ and $\sigma_{em} = 700\ cm^{-1}$. The comparison of the experimental and simulated spectra is shown in the following figure.

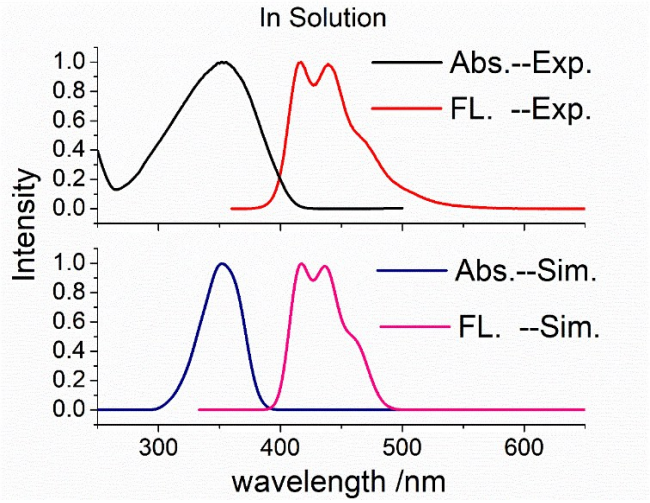

Figure S7. Simulation of spectra in solution.

2.2 Simulation of aggregate spectra

With the parameters obtained in the subsection above now we can simulate the absorption and emission spectra of aggregates with determined size. We calculated the spectra of several aggregates, and found that the following one matches the experimental results very well.

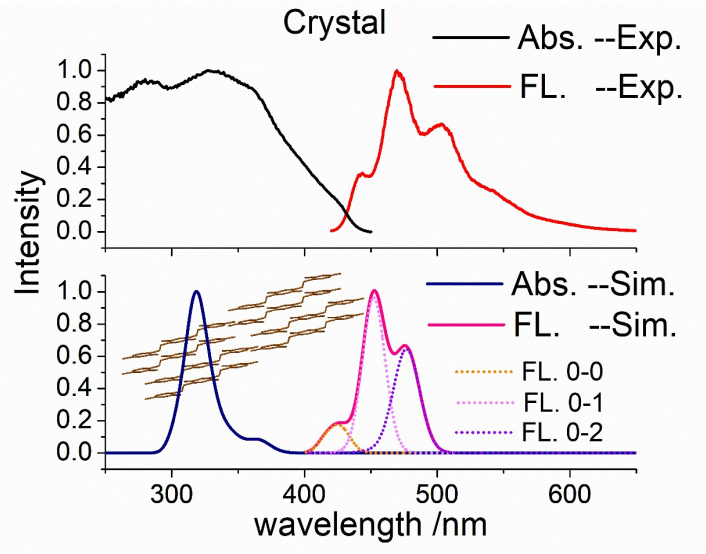

Figure S8. Simulation of spectra of aggregate. (The structure is illustrated in the same figure).

The aggregate is made of 8 molecules, 2 layers in c direction, and 4 molecules in ab direction. Between molecules in the same layer, the coupling is positive, leading to H-aggregate effect. While between the different layers, the coupling will be negative, which generates J-aggregate effect. For the emission, only the 0-0, 0-1, 0-2 components of fluorescence were computed. Almost all the spectral characters were captured by the simulated spectra. Because the calculation of 0-0, 0-1 and 0-2 peaks of fluorescence were calculated separately, here we certainly assure that the first three peaks in FL spectra were designed correctly.

2.3 Failure of dipole-dipole interaction method

As a comparison, if we calculate the spectra with just lower level dipole-dipole interaction method, then the result is shown in the following figure.

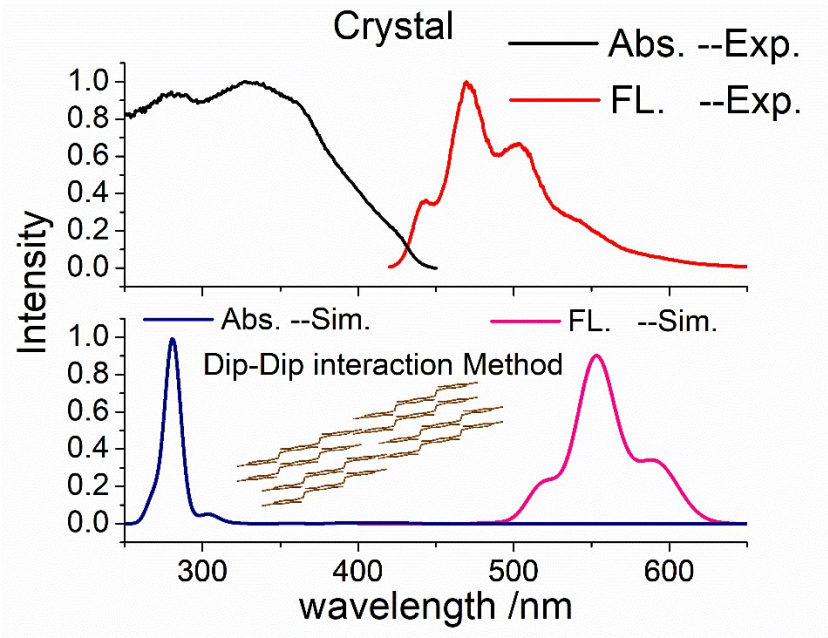

Figure S9. Simulation of spectra of aggregate with couplings all from dipole-dipole interaction method.

The simulated spectra do not match the experimental spectra as well as above results, too blue-shift for absorption, and too red-shift for emission. This is because that the dipole-dipole interaction method will overestimate the coupling between neighbored molecules. For example, the coupling of 0.072 eV will be 0.635 eV. The much larger couplings lead to the overmuch shift of simulated spectra.

2.4 Role of J-aggregate interaction

As the coupling strength tells, the H-aggregate couplings in *ab* direction are much more than the J-aggregate couplings in c direction. To evaluate the effect of J-aggregate, we calculate the following aggregate, which is consisted of just 4 molecules inside the *ab* direction. As a result, in this aggregate there is no J-aggregate coupling. The spectra are shown in the following figure.

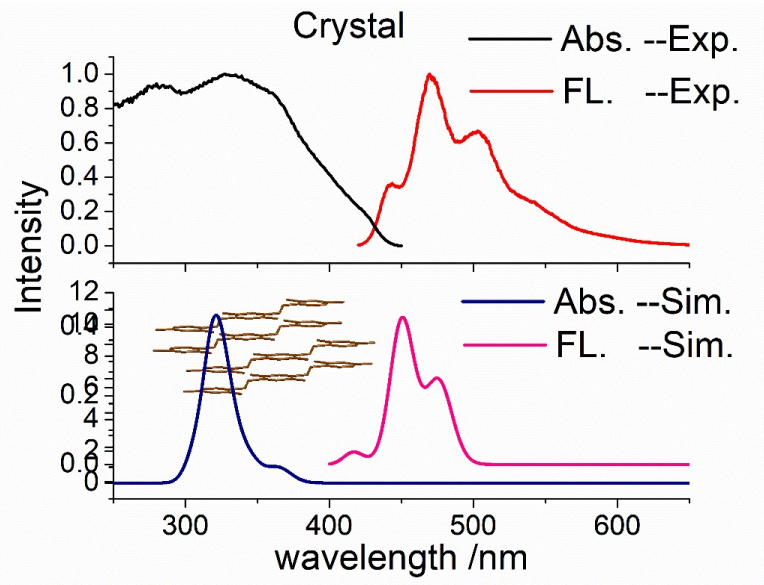

Figure S10. Simulation of spectra of smaller aggregate with only H-aggregate effect inside the ab diretion.

As we can see, the absorption spectra changes just a little comparing to the ones in Figure 2d, confirming that H-aggregate effect is dominant. However, the obviously smaller 0-0 peak in FL spectrum implies that J-aggregate effect is not ignorable.

References

1. Hsu, C. P., The Electronic Couplings in Electron Transfer and Excitation Energy Transfer. *Acc. Chem. Res.* 2009, 42 (4), 509-518.
2. Krueger, B. P.; Scholes, G. D.; Fleming, G. R., Calculation of couplings and energy-transfer pathways between the pigments of LH_2 by the ab initio transition density cube method. *J. Phys. Chem. B* 1998, 102 (27), 5378-5386.
3. Spano, F. C., The Spectral Signatures of Frenkel Polarons in H- and J-Aggregates. *Acc. Chem. Res.* 2010, 43 (3), 429-439.
4. Spano, F. C., Analysis of the UV/Vis and CD Spectral Line Shapes of Carotenoid Assemblies: Spectral Signatures of Chiral H-Aggregates. *J. Am. Chem. Soc.* 2009, 131 (12), 4267-4278.

F. Setup of the Micro-PL (μ-PL) System.

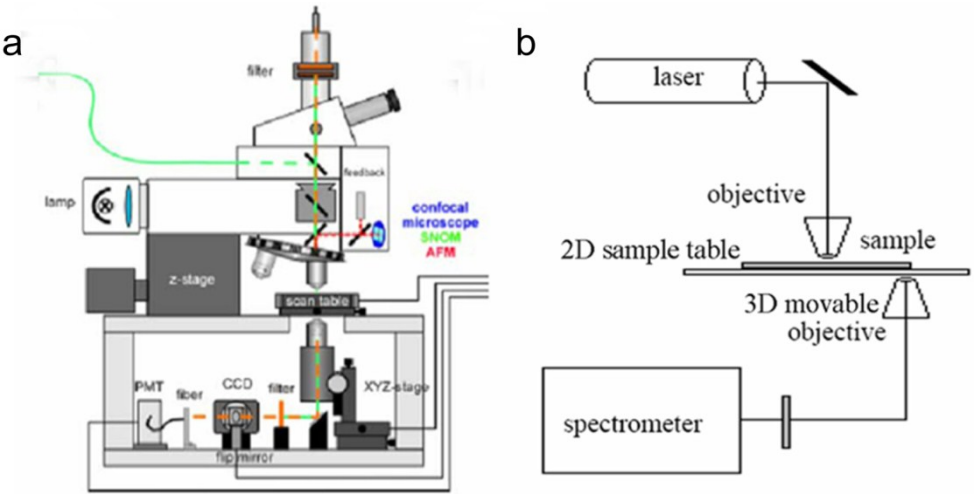

Figure S11. Schematic illustration of (a) the near-field scanning optical microscopy, and (b) the transmittance optical path for the waveguide measurements.

Individual 6M-DSB miroribbon was investigated at room temperature in air by a home-made optical microscopy equipped with a 50 × 0.9 NA excitation objective. The second harmonic (400 nm, 150 fs, 1 kHz) of a regenerative amplifier (Spitfire, Spectra Physics) seeded with a mode-locked Ti:sapphire laser (Tsunami, Spectra Physics) was focused to a 40-μm-diameter spot to excite the selected individual part of microribbon along the width direction. Then PL spectra were collected underneath by using a 50 × 0.9 NA objective that was mounted a 3D movable stage. A 420-nm long-wave pass dielectric filter was used to block any scattered excitation light. Finally the collected PL was coupled to an optical fiber with diameter 25/125 μm (core/cladding) and detected using a liquid-nitrogen-cooled CCD (SPEC-10-400B/LbN, Roper Scientific) attached to a polychromator (Spectropro-550i, Acton). The spectral resolution is 0.1 nm. Using the same detection geometry, time-resolved PL was detected with a streak camera (C5680, Hamamatsu Photonics) dispersed by a polychromator (250is, Chromex) with a spectral resolution 1 nm and a time resolution 10 ps. Figure S11b is a representative of our setup.

G. Preparation of concave PDMS microgroove template pad.

In our experiments, a silicon master-template consisting of convex vertical-plates was designed and prepared by photolithography. Then Slygard 184 PDMS prepolymer (Dow Corning) was well mixed and casted on the silicon master-template. After incubating at 343 K for 4 h, the PDMS pad with a thickness of about 0.5 cm was peeled off the master and was cut into 1×1 cm² prior to use. The dimensions of microgroovs on the PDMS pad were determined by those of convex silicon vertical-plates. Typical PDMS-RGTs used in this study have a width of ~2 μm, a height (or depth) of ~5 μm, and a length 50 μm (Figure S12)

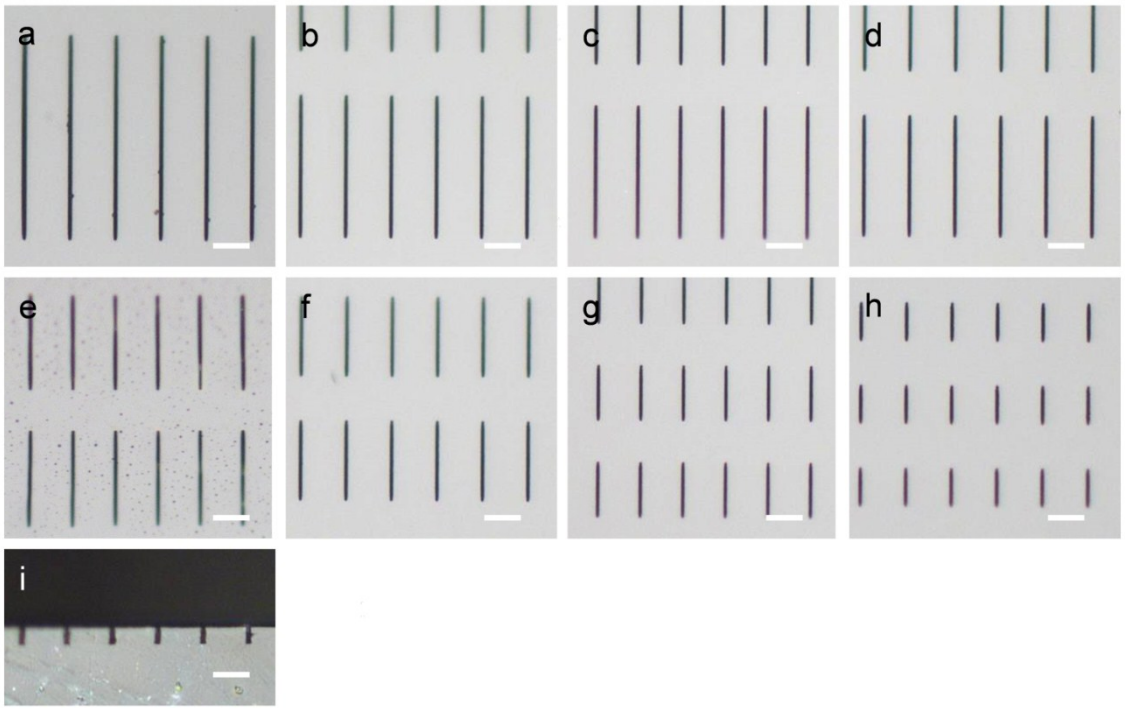

Figure S12. Bright field microscopy images of PDMS-RGTs with different lengths and spacings. (a-h) viewed from the front-surface of PDMS-RGT pad and (i) from the cleaved side-face of PDMS-RGT pad, respectively. Scale bars, 10 μm. The lengths of RGTs are 50, 40, 35, 30, 25, 20, 15, 10 μm for images a-h, respectively. The depth of all groove is 5 μm.